Testing and Analysis of Q-Weak's Multiplexing Electronics System

A thesis submitted in partial fulfillment of the requirement for the degree of Bachelor of Science in Physics from the College of William and Mary in Virginia,

by

Ryan B. Zielinski

May 6, 2010

Abstract

The Q-Weak experiment, which will run at Thomas Jefferson National Laboratory beginning in summer 2010, is a precision test of the proton's weak charge using parity-violating electron scattering. Q-Weak will place new constraints on the running of the weak coupling; any deviation from the current Standard Model prediction could signal new physics. Q-Weak employs four vertical drift chambers, each consisting of two wire planes of 280 wires, in a U - V arrangement to complete the path reproduction of incident electrons. A multiplexing system will allow for the determination of both the position and drift time of the path. The goal of this project was to test the time resolution, signal integrity and signal stability of the multiplexing electronics associated with the data readout of the four VDC's. This was done by performing four tests. First, all the wires in a single vertical drift chamber were read out through the multiplexing electronics. From this data, maps were created that mapped the time response of signals in the electronics. From these maps, we were then, secondly, able to demultiplex the data and assign individual wires time-windows on given TDC channels. This allowed us to calculate seven-track wire efficiencies. The final two tests both dealt with characterizing the multiplexing electronics crate. One test determined the thermal response of the crates. This means that we checked signal stability as the crate was powered on and over a 24 hour data taking run. The final test to determine whether there was a time window, within which multiple signals could arrive on a given delay chip that resulted in a shifted time spectrum.

Contents

Chapter 1

Introduction

The Standard Model of Particle Physics describes the interactions (via force-carrying bosons) of the six leptons and six quarks that make up the basic building blocks of matter. An incredibly successful theory, it correctly predicts the masses of all known elementary particles. The Standard Model also correctly predicted the existence of the weak gauge bosons, gluon and top and charm quarks before they were observed experimentally. Furthermore, every high-energy physics experiment run since the theory's inception has found agreement with it. Even despite this remarkable consistency between theoretical predictions and experimental results, the Standard Model of particle physics is known to be incomplete. Developed initially as a description of the electromagnetic and weak forces, the theory also incorporates the strong nuclear force. Unification, however, with the fourth fundamental force, gravity, has remained elusive. The theory further fails to take into account cosmologically observed dark matter and energy and also cannot explain the relative weakness of gravity (by comparison the weak force is 10^{32} times stronger).

The incomplete nature of the Standard Model has led physicists to search for physics beyond the scope of the current theory. Experimental physicists tackle this in two ways, through low and high-energy experiments. High-energy experiments, such as those at the Large Hadron Collider, collide particles at ultra-relativistic speeds in an attempt to create new forms of matter. Low-energy experiments are precision measurements of the Standard Model's predicted parameters. Discrepancies between predicted and measured

values would indicate either new fundamental particles or forces in nature. One such low energy experiment will begin in the summer of 2010 at Jefferson Laboratory. Q-Weak will use the CEBAF accelator to probe the electroweak interaction. This low energy test of the Standard Model will measure the weak charge of a proton and its constituent quarks, for which a value is predicted within the Standard Model.

The purpose of my research was to test the multiplexing electronics system that is used to read out data from Q-Weak's vertical drift chambers. In the experiment, the vertical drift chambers (which are gas-filled wire chambers) allow for position and momentum measurements of the elastically scattered electrons, as well as electron-track reconstruction. The multiplexing electronics system was developed at Jefferson Laboratory and preliminary tests were run on it there. These tests confirmed the basic operation of the system. My task was to elaborate on these initial tests and check the signal stability, signal integrity and thermal response of the electronics.

I also used the multiplexing electronics as a further diagnostic test on the vertical drift chambers. Analysis of the data that the system read out, from the chambers, was used to map the time response of sense wires inside the chamber. The data was also analyzed to infer wire efficiency.

Chapter 2

The Q-Weak Experiment

2.1 Q-Weak Overview

Q-Weak will scatter 85% polarized electrons at 1.165GeV off of a 35cm long liquid hydrogen target. The aim is to measure the weak charge of a proton and its constituent quarks, through parity-violating electron-proton scattering. Measurements will take place at very low momentum transfers $Q^2 = .03\ (GeV/c)^2$. Low four-momentum squared values minimize the size corrections due to the proton's size. The weak charge then becomes the sum of the charges of the two up and one down quarks. The experiment will be highly precise with a combined stastical and systematic error of approximately 4%, as show in Figure 2.1.

2.2 Parity Violation

A parity operation is similar to a mirror reflection. In an orthogonal three dimensional coordinate system, the coordinates x,y and z would change to -x,-y and -z under a parity operation. Physicists originally believed that fundamental physics would remain unchanged under such a transformation. Such interactions are said to be parity conserving. However, in 1957 it was demonstrated that the interaction responsible for the beta decay of a Cobalt-60 nuclei did not conserve parity. More specifically, it was found that in the decay the nuclei emitted more electrons with a -z component of momentum

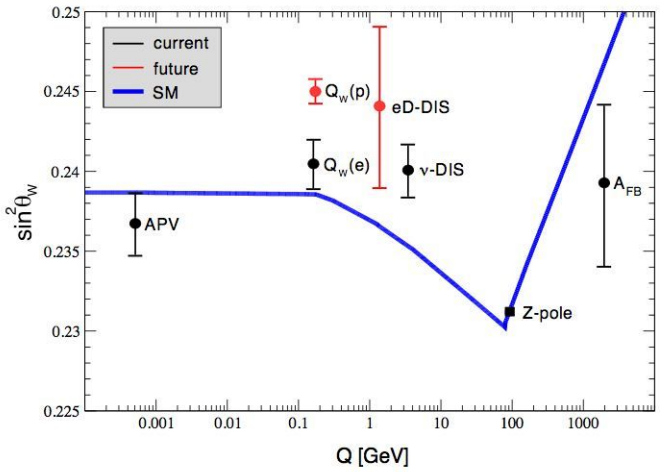

Figure 2.1: A figure illustrating the running of $sin^2\theta_W$ as a function of the momentum transfer Q(GeV/c). SM (blue) is the Standard Models prediction. Black points denote previous measurements that have been made. Red points denote future measurements in planned experiments. The error bars on the red points indicated the anticipated level of precision.

than a +z component. This can be explained if an interaction depends on the screw-like behavior of particles. This is demonstrated in Figure 2.2 [1]. If this behavior is an intrinsic property of the particles, such as spin alignment (handedness) then this leads to parity violating physics.

2.3 Theoretical Background

A fundamental parameter contained within the Standard Model is the weak mixing angle, $sin^2\theta_W$, and it is related to the weak charge of the proton by the relation

$$Q_W^P = 1 - 4sin^2\theta_W. \tag{2.1}$$

The Standard Model defines this mixing angle as the ratio between the masses of the weak force mediating bosons such that

$$cos^2\theta_W = \frac{(M_W^2)}{(M_Z^2)}. \tag{2.2}$$

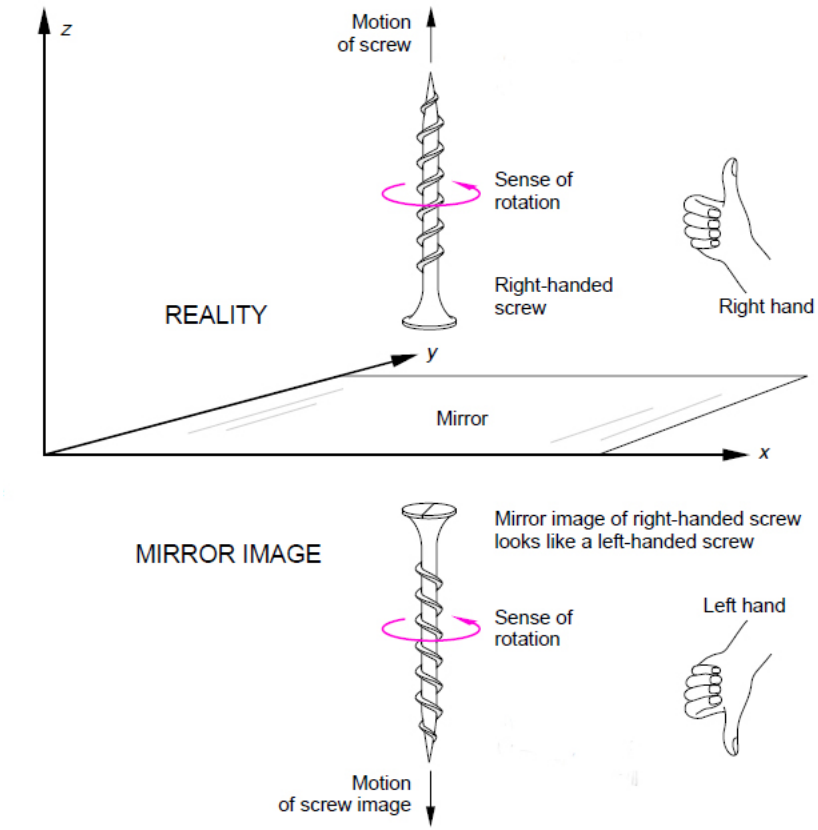

Figure 2.2: This figure is an explanation of how screw-like behavior does not conserve parity. The top screw has right-handed threads. When it is rotated, it advances in the +z direction (up, in the figure). Its mirror image, however, has left-handed threads. Further, as the screw rotates, its mirror image rotates in the same direction but advances in the -z direction. Parity is not conserved.

The ratio can be described further as the "mixing" of the electromagnetic and weak interactions. At energy scales above that of the rest energy of the Z boson, Z boson exchange is comparable to a photon exchange in an electromagnetic interaction. The Standard Model makes its prediction of the weak charge of a proton based on the weak mixing angle. In fact, it makes its prediction based on the variation of the weak mixing angle as a function of momentum transfer. In other words, the proton's weak charge is sensitive to the weak mixing angle such that a low energy (low 4-momentum squared transfer, Q^2) experiment is useful in determining its value.

2.4 The Weak Interaction

The weak interaction is mediated by the W and Z bosons. The three bosons, W^+, W^- and Z^0 have charges of +1, -1 and 0 respectively. Due to the nature of their charge each boson acts differently depending on the spin orientation of the fermions they interact with. The W^+ boson only acts on a fermion with spin parallel (right-handed) to its velocity. The W^- boson only acts on a fermion with spin anti-parallel (left-handed) to its velocity. The Z^0 boson, because of its electric neutrality, acts on both types of fermions but with varying magnitude. This unique property of Z^0 bosons leads to an inherent asymmetry in the probability of left and right handed fermion scattering [2]. Q-Weak will use this fact to measure the weak charge of the proton.

2.5 Asymmetry

In charged particle elastic scattering, W boson exchange is not allowed through conservation of charge. This leaves the scattering interaction to be mediated by two force particles, the photon for the electromagnetic force and the neutral current Z boson for the weak force. When a photon is exchanged in the electromagnetic interaction it does so with equal magnitude in regards to both fermion spin orientations. Therefore, the electromagnetic force will not contribute to the asymmetry in the electron scattering. The asymmetry is then defined as

$$A = \frac{\sigma^+ - \sigma^-}{\sigma^+ + \sigma^-}, \tag{2.3}$$

where σ^+ and σ^- are the scattering cross sections of the right and left handed fermions under an elastic collision. Quantum Field Theory shows that this asymmetry should also be defined by (as a low order approximation and at low 4-momentum squared transfers) [3]

$$A = \frac{1}{P}\frac{-G_F}{4\pi\alpha\sqrt{2}}\, Q^2 Q_W^P, \tag{2.4}$$

where P is the polarization of the electron beam, Q^2 is the four-momentum transfer, G_F is the Fermi coupling and α is the fine structure constant. For low enough momentum transfers, higher order structural terms can be ignored in Eq 2.4. The size of these proton-structure dependent terms have been sufficiently constrained in higher Q^2 experiments. Ignoring these higher order structural terms is valid because low energies are unable to provide enough resolution to "see" their effects. Q^2 values will be determined experimentally as a function of the scattering angles used.

2.6 Experimental Setup

After the longitudinally-polarized incident electron beam hits the liquid hydrogen target, a magnet is used to bend scattered electrons away from the beam. The scattered electrons then pass through a series of collimators to select a scattering angle of 9 +/- 2 degrees and a corresponding Q^2 of .03GeV^2 [4]. A toroidal magnet then bends the scattered electrons away from the beam line at different angles due to their different momentums. This is shown in Figure 2.4 [4]. Electrons with the correct momentum are focused onto eight quartz Cerenkov detectors. Scattered electrons excite electrons in the quartz dielectric and when the excited electrons return to their ground state they emit a photon. The emitted photons are detected by photomultiplier tubes connected to the Cerenkov bars. Cerenkov bars hold the distinct advantage of being insensitive to low energy particles and thus particle detection remains relatively insensitive to the cosmic-ray background.

The experiment will run in two separate modes, tracking (calibration) mode and data production (high-current) mode. The tracking mode will run first to determine the response of the quartz detectors, the four-momentum transfer, and error associated with inelastically scattered electrons entering the detectors. The tracking mode is characterized by a low count rate that allows for the reconstruction of individual scattered electron tracks, through the suppression of Møller scattering. In the high-current data-production mode, the tracking system chambers and trigger scintillators will be

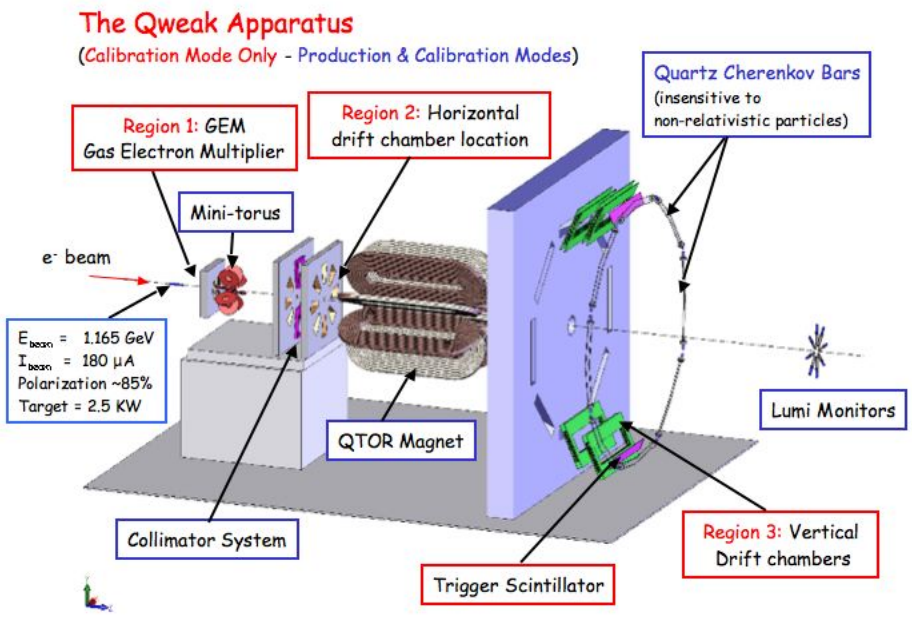

Figure 2.3: The Q-Weak Tracking System will consist of three regions. The College of William and Mary is responsible for the region three drift chambers. In production mode the chambers will be retracted into special shielding huts (not pictured) to protect them from the beam line. The experiment will shift between production mode and calibration mode throughout the duration of the experiment. The eight slots in the collimator correspond to the eight segment toroidal magnet and the eight Cerenkov quartz detector bars.

retracted to prevent damage. The high-current mode is when the asymmetry measurements will occur.

The tracking system's experimental set up can be seen in Figure 2.3. In tracking mode scattered electrons will go through a three region tracking system before entering the quartz detector bars. The tracking system will be responsible for reconstructing the particle's path. Each region serves as a filter for inelastic, secondary, and electron-electron scattering events. Different types of scattering are sorted by their physical signatures such that only elastically scattered electron become the basis for calculations. Region I is responsible for determining the position of the electrons as they scatter from the target. This region will consist of Gas-Electron Multipliers (GEM's). Region II will determine the position of the scattered electrons before they enter the torus shaped

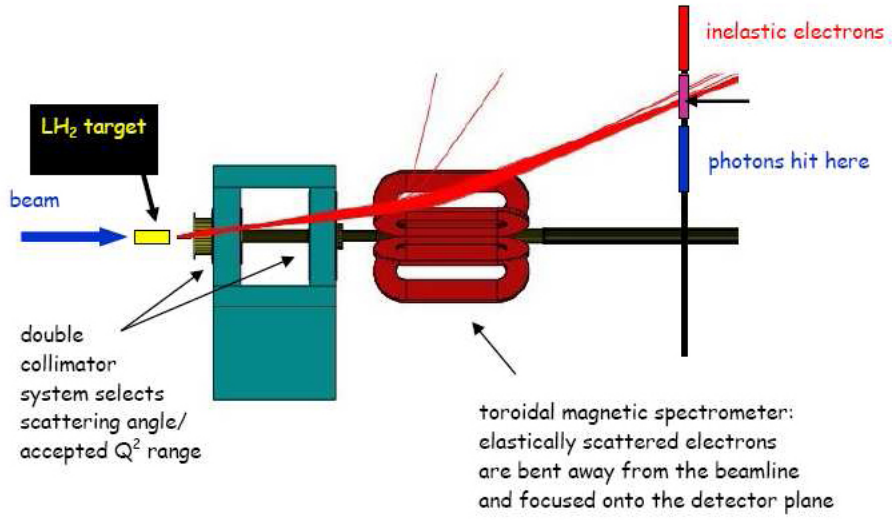

Figure 2.4: This figure shows the collimator and magnet set up. Region I is before the double collimator and Region II is immediately following it. The red track describes the path of the elastically scattered electrons.

magnet and are bent away from the beam line. This region will consist of horizontal drift chambers as well as the QTOR toroidal magnet. Region III will make certain that only elastically scattered particles are entering the quartz detectors. It will determine the position, angle, and momentum of the particles. In order to do so, this region will consist of four vertical drift chambers assembled on a rotating chassis to accommodate the entire detector system. To cover the eight octants necessary four measurements will need to be made because, as shown in Figure 2.5, only two octants are measured at a time. This region will also include a trigger scintillator to provide a trigger for the read-out electronics and a timing reference during the tracking mode.

The asymmetry described by equations 2.3 and 2.4 is predicted to be only .23 ppm and as such measurements are sensitive to experimental conditions. For example, a voltage fluctuation in the gain electronics of the photomultiplier tubes could be enough to create false asymmetries (even if it only occurred in a part per ten thousand). To eliminate these errors the polarization of the incident beam will be switched as many as 500 times a second. Building on the previous example of voltage fluctuations, the belief is that by switching the beam at a fast rate both left and right handed electrons will

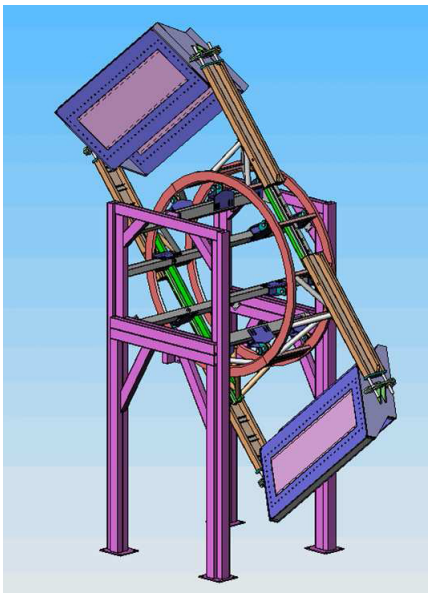

Figure 2.5: The drift chambers are placed at opposing octants so that two measurements can be made at a time. A total of 4 measurements will need to be made in order to cover the entire detector system.

experience the same experimental variations, eliminating a potential source of error.

2.7 The Drift Chambers

A drift chamber is a gas-filled cell, containing an array of wires and a high electric field to detect charged particles [5]. The wires are held at ground and the high electric field is applied to the cell. Particles that pass through the cell ionize the gas and free electrons. These free-electrons drift towards the grounded sense wires. By measuring the drift time of the freed electrons both the location and angle of the primary particle can be determined. The drift time is defined as the time for the first electron to hit the detector wire and, similarly, its velocity is the drift velocity. In total each chamber used, in the Q-Weak experiment, will contain an array of 560 wires spaced at 5 mm and strung diagonally in a U-V plane arrangement. Two wire planes oriented at 153 degrees to each other (280 wires each) are used to make sure all particles are detected.

Elastically scattered electrons enter the drift chamber and collide with the gas molecules creating molecule-electron ionization pairs. The freed electrons become accelerated towards the grounded wires by the large electric field within the chamber.

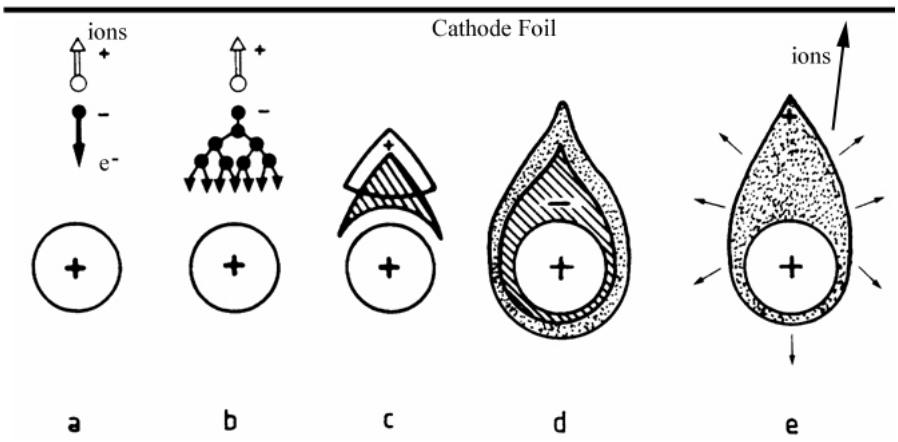

Figure 2.6: This figure demonstrates the avalanche effect (time development). At (a) the primary electron travels towards the grounded sense wire. On its way to the wire the electron, due to the increasing electric field, undergoes more ionizing collisions (b). The avalanche begins to develop (c) and as more electrons are rapidly collected (d) the remaining cloud of positive ions is stretched out towards the cathode (e).

The closer to the grounded wires the freed electrons get the larger the electric field, and with this the acceleration, becomes. The increased acceleration and energy allow for the creation of more electron-ion pairs; this is known as the avalanche effect and is shown in Figure 2.6 [6]. The avalanche effect leads to a signal on the sense wires. Knowing the drift distances for several wires allows for the path reconstruction of the elastically scattered electrons.

In order to keep the drift velocity as stable as possible a mixture of Argon (65%) and Ethane (35%) gas is used. Although any ionizable gas can be used, noble gases provide avanlanche multiplication at lower electric fields and therefore are used as the main component of the gas mixture. A polyatomic molecule such as ethane is used as a quencher. Due to the large number of non-radiated states in such molecules they absorb secondary emissions that would otherwise create spurious avalanches. Secondary emission occurs as the ions approach the cathode foil and gain an electron from it. In this process either a photon is emitted or an electron is re-emitted [7].

2.7.1 Vertical Drift Chambers

The Q-Weak experiment will employ a specific kind of drift chamber known as a vertical drift chamber. As the name implies, a vertical drift chamber determines the path of an elastically scattered electron by creating ionization that occurs in the vertical direction (see Figure 2.7. This vertical drift is achieved by applying a high negative voltage to the chamber. Positively charged ions drift towards the cathode planes of the chamber while negatively charged electrons drift towards the grounded wires. Working backwards, knowing the relationship between the time and perpendicular distance to the grounded wire, the position of the primary electron can be determined.

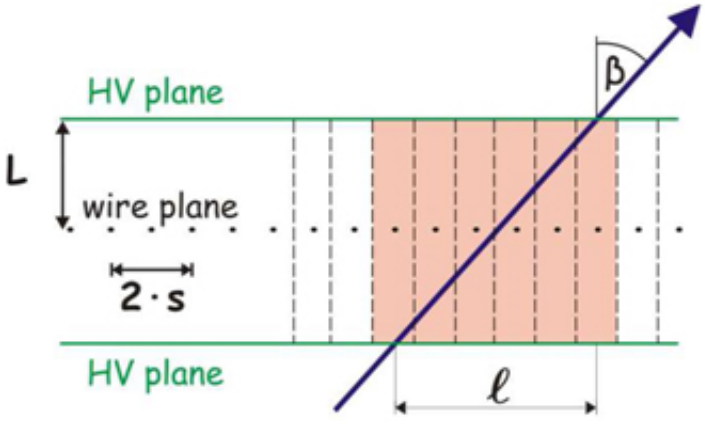

Figure 2.7: A diagram of the vertical drift chamber found in Region III. The top and bottom lines are the high voltage cathode planes. The black dots are the sense wires. The red region denotes the ionization region from the incoming blue track. L is the distance from the wires to the high voltage plane. l is the length traversed by the electron from when it enters and exits the chamber with β being the exit angle.

Chapter 3

Data Acquisition

3.1 Acquisition overview

There are four main steps to data acquisition and data analysis as shown in Figure 3.1. First a particle enters the drift chamber and ionizes the gas. The avalanche effect creates an analog pulse on a sense wire. The analog pulse is then amplified and discriminated as it is read out from the drift chamber and into the multiplexing electronics crate. When the particle exits the drift chamber it passes through and creates a signal on the trigger scintillator. Second, the VME-standard multiplexing crate combines multiple signals from separate wires in the chamber onto pairs of output channels. The reason for this will be explained further in the paper. Third, the output from the multiplexing crate is fed into a time to digital converter (TDC). The signal from the trigger scintillator is also fed into the TDC and is used as a timing reference. Fourth, the output of the F1TDC is hooked up to a PC where the data can be recorded and analyzed with a computer.

3.2 Drift Chamber Readout

From the chamber, wire data is read out through 16-channel amplifier discriminator circuit boards known as MAD boards. Each channel on a MAD board corresponds to a wire in the chamber. There are a total of 36 circuit boards (18 per plane) to read out an entire chamber's worth of wires. The MAD boards output a low-voltage differential

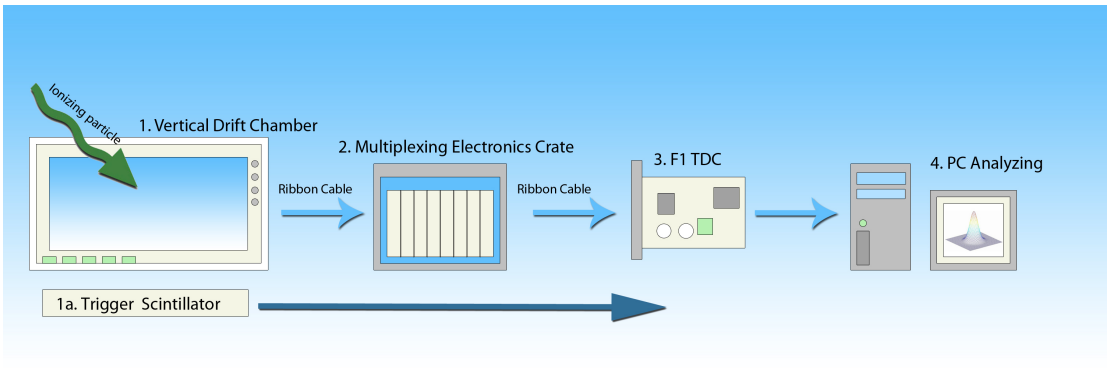

Figure 3.1: This figure shows the process of data acquisition.

signal (LVDS) to help suppress noise.

The sense wires are strung diagonally through the wire planes. This results in differing wire lengths based upon wire number. The shortest wires occur at the ends of the plane and the longest occur in the middle. The configuration of wire assignment to MAD board can be found in Figure 3.2. A quick multiplication of the channel number per board and number of boards shows an extra factor of 8 channels per plane. To account for this there were eight dead channels per plane of data and these channels were located on the #10 MAD board.

The MAD board outputs its data on twisted-pair ribbon cables. The cables would then ideally be fed into a TDC channel for analyzing, but as previously mentioned each drift chamber contains 560 sense wires. Summing over the four chambers it becomes apparent that a total of 2240 wires need to be read out and analyzed. Assuming an individual TDC channel is assigned to each wire and a 64 channel TDC is used, 35 individual TDC's would be needed to handle the data load. To save on this considerable expense a multiplexing system consisting of multiple delay lines was implemented. In the system, 18 wires from separate locations in the chamber are placed onto two signal paths leading into two TDC channels. From the sum of the two signals the drift time can be determined and from the difference of the two signals the triggered wire can be identified. This process reduces the number of TDCs needed by a factor of nine.

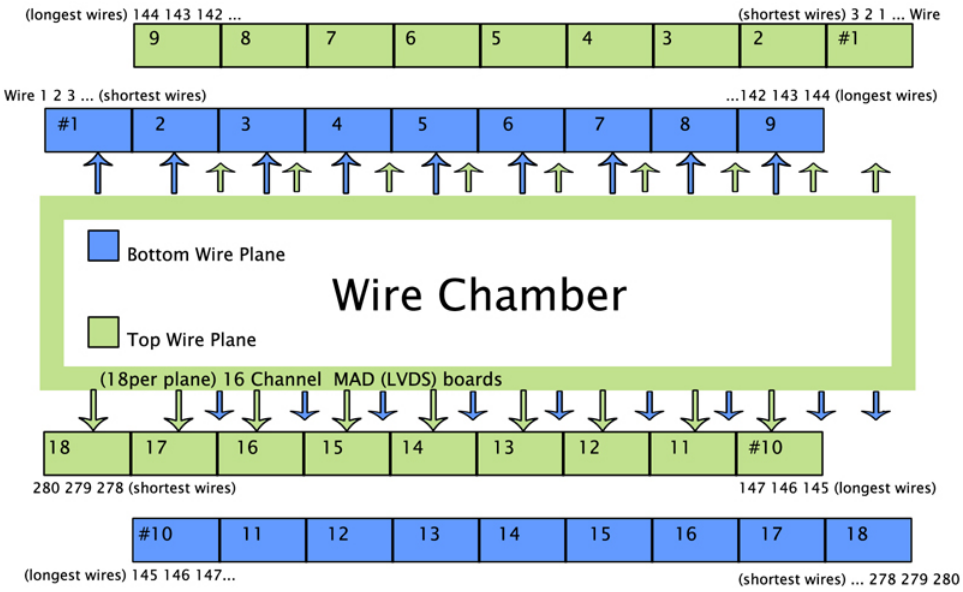

Figure 3.2: This figure shows the implementation of the wire read-out from the drift chamber. The drift chamber is a rectangle in which the sense wires are strung diagonally resulting in a differing length for each wire. Each color corresponds to a wire plane where half a plane is read out per side of the chamber. Each MAD board channel corresponds to wire from the chamber. For example, the MAD board labeled #1's first channel would output data from the first wire in that plane, the second channel would output data from the second wire and the second MAD board would start with the seventeenth wire.

3.3 Multiplexing Implementation

3.3.1 Delay Line Scheme

The delay scheme is based on simple ECL logic in which OR gates act as the delay mechanism. Once the wire signals leave the drift chamber they are split into the delay line consisting of the logic gates. One signal will go "left" and the other will go "right". The delay scheme delays every 9th wire by 1.3 ns, meaning every 9th wire is multiplexed into a single delay line where the signals are offset by 1.3 ns. The split and delayed signals are then read out on the left and right side of the delay line where the difference (left minus right) can be taken to determine which wire was hit. The delay is provided by a MC10H188 (Figure 3.4) high-speed Hex Buffer chip. Multiple MC10H188 chips are connected together to create a single delay line (see Figure 3.3).

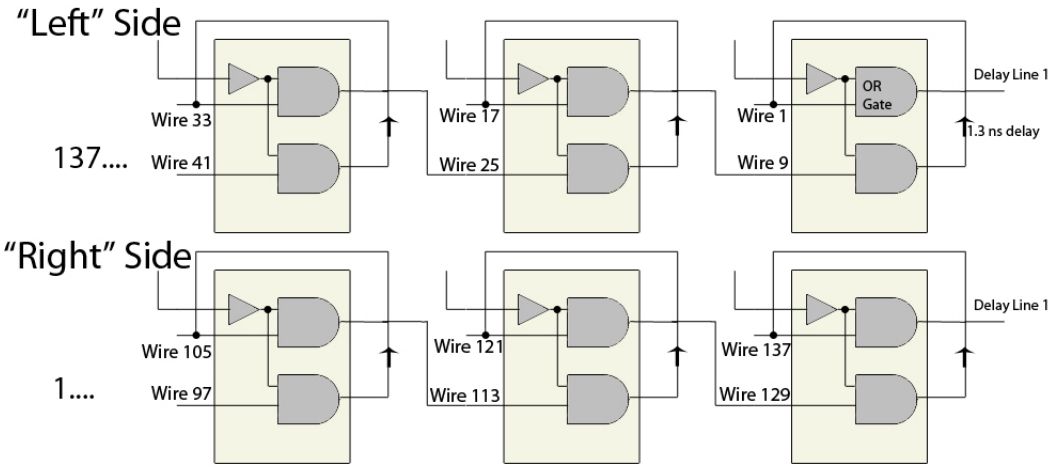

Figure 3.3: This schematic shows the left and right sides of a delay line and how multiple HEX buffer chips are connected to produce a delay line. This cartoon depiction only shows two OR gate delays per buffer when the actual chips take inputs from six wires.

3.3.2 Multiplexing Crate

The LVDS signal created by the MAD boards is fed into the external multiplexing (MUX) crate, Figure 3.5. The crate turns the LDVS signal into an ECL pulse via the LEX2 boards developed at Jefferson Lab. As an ECL pulse the signal from the LEX2

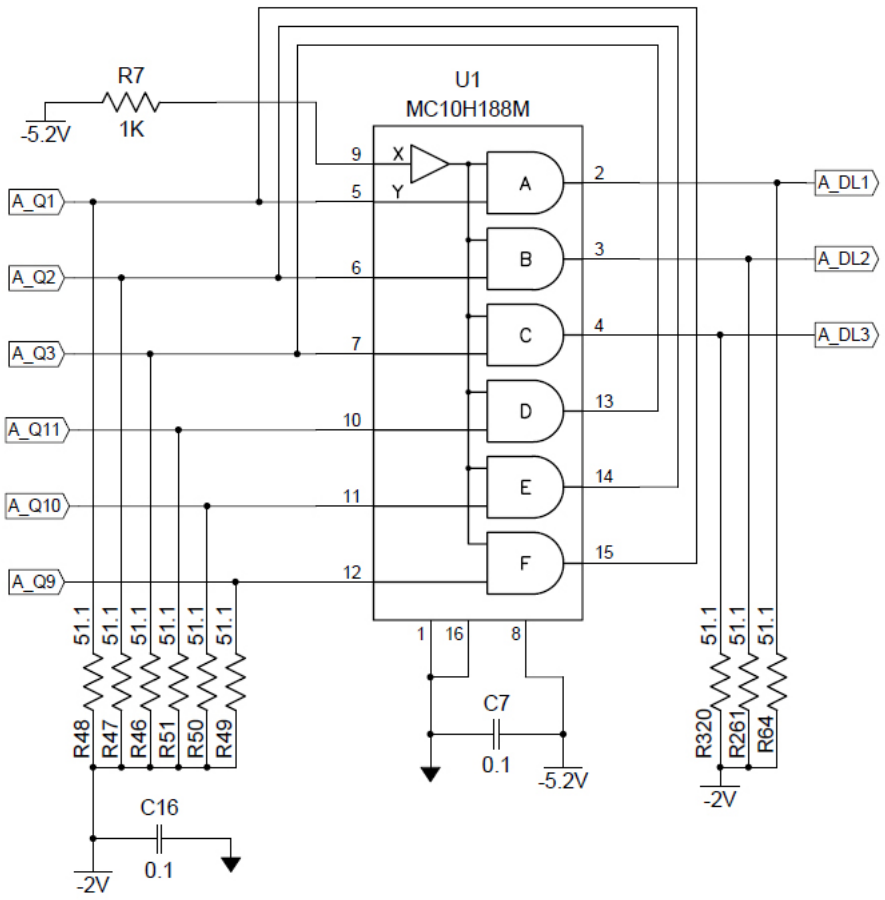

Figure 3.4: The MC10H188 delay chip. The OR gates are constantly on/enabled.

boards is split and then fed into the ECL-gate delay-backplane. The LEX2 boards are connected to this backplane. Technical jargon aside, when a wire is hit in the chamber, it will be read out as previously described and into the multiplexing crate. Once the signal reaches the crate it will be fed into to the delay mechanism where it is split. Each pair of corresponding TDC channels (i.e 0 and 1) correspond to a certain set of wires (i.e. 1, 9, 17...). The left minus right subtraction is done on a channel pair basis (i.e. TDC0 - TDC1). Depending upon the time location of the signals within each channel pair, the hit wire can be determined. Each wire within a delay line can be thought of as having its own time signature. For example, the first wire in each channel will experience no "left" delay but the maximum "right" delay as it will pass through every

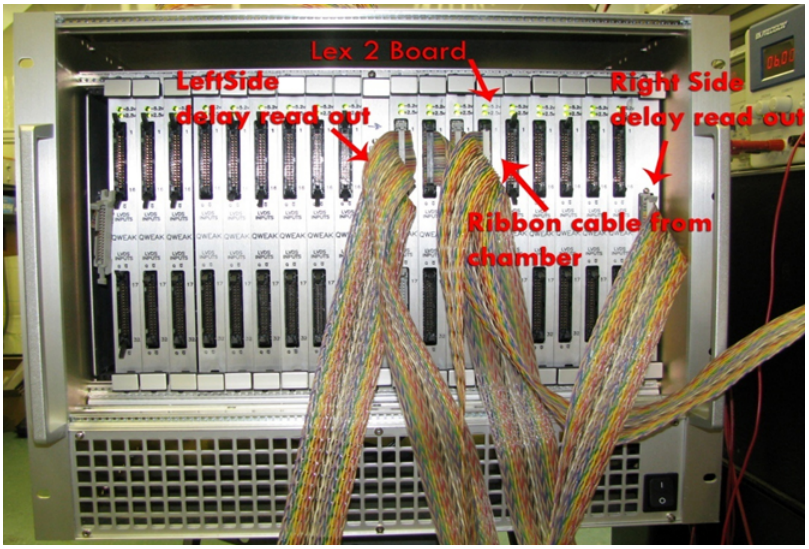

Figure 3.5: This figure shows an actual photograph of the experimental MUX.

possible delay gate. This results in a maximally negative signal location in the time spectrum. The second wire of the input channel will pass through 1.3 ns more of delay on the "left" and 1.3ns less of delay on the "right" shifting this wire signal 2.6 ns to the right of the first signal in the time-signal spectrum. More precisely the first wire will be the first signal in the time spectrum and the second wire will be the second signal in the time spectrum. Building this up wire by wire it becomes apparent that a total of up to eighteen signals should be seen per channel pair (as a maximum of 18 wires are feed into a single delay line) and because of the left minus right measurement the separation between the signals should be 2.6 ns. A diagram of this concept is shown in Figure 3.6.

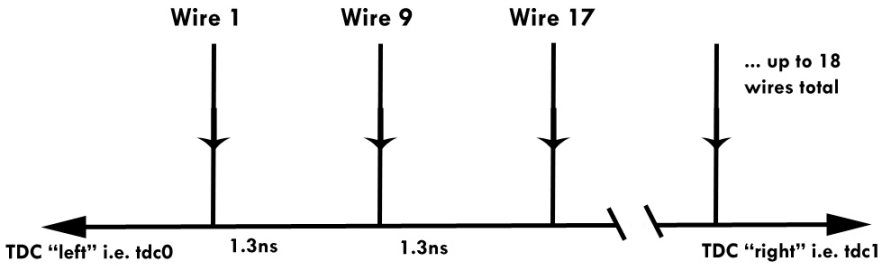

Figure 3.6: Concept of the delay line technique. The diagram is repeated for each set of TDC channels. For example, the schematic for TDC2 and TDC 3 would contain wires 2, 10, 18 and so on.

In order to ensure that the peak location and wire assignment remained valid through multiple runs of data, a cabling scheme was developed to ensure that the ribbon cables from the chamber were always read out in the same manner. The schematic for this can be seen in Figure 3.7.

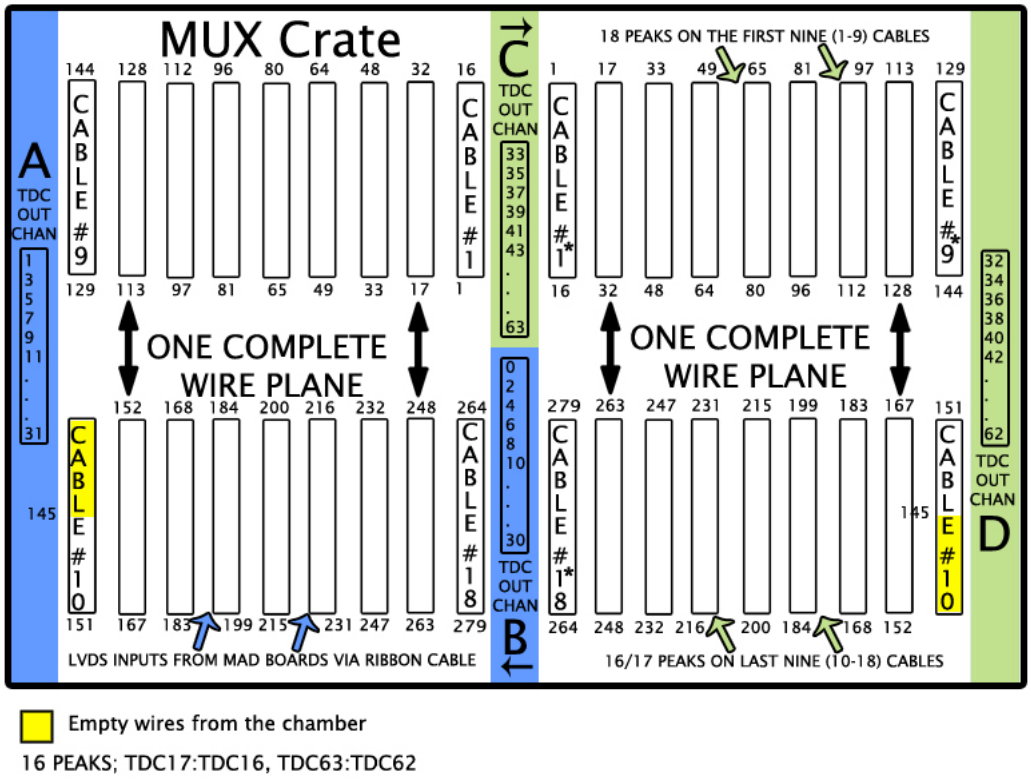

Figure 3.7: MUX crate schematic. The numbers above and below the connectors correspond to wire numbers from the chamber. Two signals per connector feed into a single delay line (every 9th wire). As previously stated one cable (#10) per plane contains 8 dead wires. This leads to TDC channel pairs that will only have 16 or 17 peaks instead of 18. A quick analysis of the delay scheme can determine the distribution of peaks. On the left side the first channel pair of the bottom connectors will have 16 peaks because as per the multiplexing scheme the 1st and 9th wire are dead. The remaining channels only have the first wire dead and thus 17 peaks. The same reasoning applies to the right side of the crate. The outputs A, B, C and D correspond to lettered connectors on the TDC.

3.4 The F1 TDC

In the experiment 64 channel F1 TDCs will be used to complete the data acquisition system (DAQ). The F1 TDC will take its inputs directly from the multiplexing crate and will output to a local PC for data analyzing. Data is recorded FIFO per channel and thus preserves the signal order described in the multiplexing scheme. In brief, the TDC records the input data in the form of data events. Data events are time windows occurring between a start and trigger signal. The start signal tells the TDC to start writing data and the trigger signal tells the TDC to "look backwards" at what was recorded during the time window. Any signals that reach the TDC within the open time window will be assigned to that event, and signals arriving outside of a time window are disregarded (see Figure 3.8). In synchronous mode the start signal is automatically generated and is programmable, allowing all the TDCs in the experiment to be synchronized together. The trigger signal is provided by the trigger scintillator.

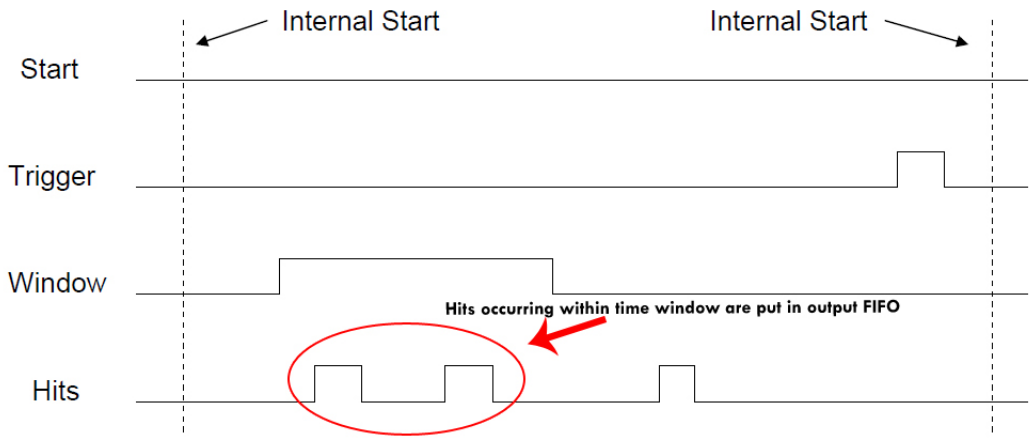

Figure 3.8: F1TDC pulse diagram showing a simulated data event. The pulses circled in red will be output because they occur within the time window. In the experiment the trigger pulse will be provided be the trigger scintillator. The scintillator will be on top of the drift chamber and will create a signal when a electron passes through it, into the chamber.

3.5 Computer Analysis

The computer data analysis model is simple. The raw data from the F1TDC are decoded and analyzed by an event-processing program on the computer(xTychoAnalysis). xTychoAnalysis data is stored in a ROOT file in the format of a event based data-tree. Each leaf of the tree corresponds to a channel of the TDC. The TDC records time in variable units called bins. The calibration on the TDC can be changed changing the time resolution of the TDC. For our purposes the resolution was set at 112ps/bin. In ROOT the left-right subtractions can be made creating signal time spectrums that allow for the data to be demultiplexed.

Chapter 4

Results

During the course of my research four main tests were run on the multiplexing electronics. These tests included mapping the time-signal spectrum of the multiplexing crates and demulitplexing the data, determining the wire efficiency of the drift chambers, and running thermal and signal delay tests on the multiplexing electronics.

4.1 Map Making

A key component of characterizing the multiplexing crates was creating a "map" relating signal number within channel pairs to individual wires within the chamber. This map allowed for individual signals to be demultiplexed into a individual wire number. In other words the map translated, based on channel number and location of the signal in the time spectrum, a signal into a physical wire in the drift chamber. Any future data run then used the map to assign wire numbers. The demultiplexed data is crucial for track reconstruction of the elastically scattered electrons and determination of Q^2. With the map clearly dependent on signal integrity, time resolution and signal stability, another key component of testing the multiplexing electronics was understanding the behavior of the signals in the crates.

Maps were created using a C/C++ script run in ROOT. In ROOT the left minus right calculations were done on a channel by channel basis to produce the signal time spectrum. The script would then identify each signal using ROOT's peak finder func-

```
Run number: C775_1132.root
Channel numbers: tdc1:tdc17
 ***************

 Peak 1
 Name            Value           Error
 Constant        87.176080       7.933803
 Mean            16.634045       0.074530
 Sigma           1.093570        0.066648

 Peak 2
 Name            Value           Error
 Constant        88.325089       7.940070
 Mean            45.819869       0.075498
 Sigma           1.049514        0.061624

 Peak 3
 Name            Value           Error
 Constant        80.456112       7.500501
 Mean            69.009664       0.079003
 Sigma           0.949084        0.051772

 Peak 4
 Name            Value           Error
 Constant        47.948118       5.714605
 Mean            -11.529989      0.079003
 Sigma           1.165938        0.093029
```

Figure 4.1: Example output of a text file

tion call. Once the signals were identified, Gaussian fits were then applied to them. Information on the fit, such as its mean and sigma along with each values associated error were output to a text file. The output of the text file could then be used to develop a map, Figure 4.1. To create the actual map a time window is created for each signal/peak. The midpoint of the window is the mean value given by the fit and the time distance to the left or right of the midpoint is given by some multiple of sigma, (usually two or three).

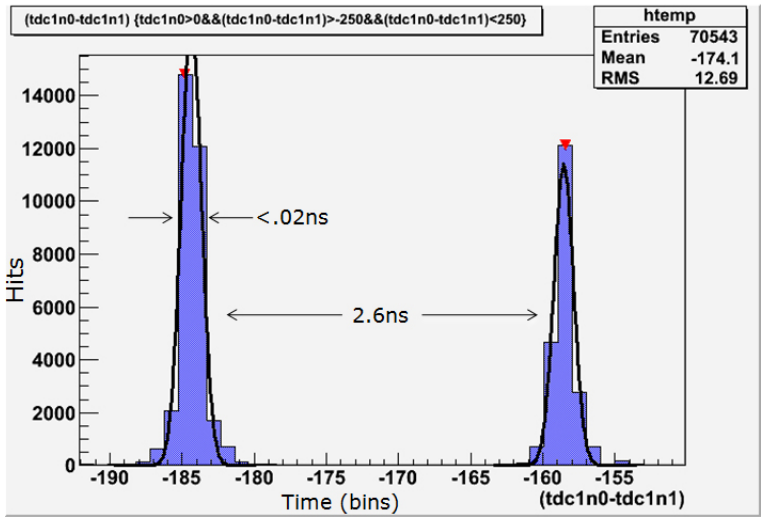

Figure 4.2: Multiplexing Verification

Prior to making maps the multiplexing electronics were tested. The electronics were

tested to confirm that signals appeared 2.6 ns apart in the time spectrum and that the width of the peaks were small enough to not create overlap with adjacent signals. These tests confirmed the time resolution of the multiplexing electronics. A example of the results of these tests are shown in Figure 4.2.

4.1.1 Cosmic Ray Maps

Initial maps were created from cosmic ray data. Cosmic rays simulated elastically scattered electrons and created signals on the sense wires in the chambers. The cosmic ray events were then read out to the multiplexing crate and TDC. A sample result from these tests is shown in Figure 4.3. A tell-tale signature of cosmic ray data is the height (number of hits) of the signal peaks. The hit rate is directly related to the position of the trigger-scintillator and the length of the wire. Regardless of the scintillator location, the smallest peaks will always be the shortest wires because cosmic rays are less likely to strike them. This allows for a quick sanity check when the map is created to make sure the right wire number is being assigned to the right peak. Another quick check is to confirm that based upon the MUX crate schematic the correct number of signals are seen on each channel pair.

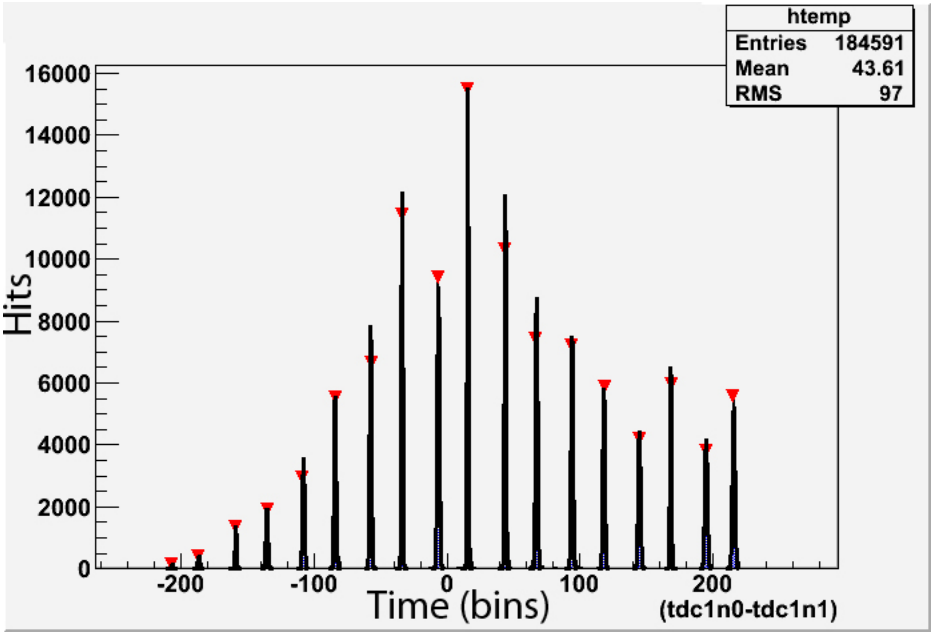

Figure 4.3: Signal-time spectrum of TDC0-TDC1 of cosmic ray data.

4.1.2 Pulser Maps

The length of data runs (more than a day) needed to obtain sufficient statistics for cosmic ray data led to the use of a pulser (PLX card) as an alternative method for creating maps. The PLX card was hooked up directly to the multiplexing crate and was able to simulate "wire hits" on the channels at once at a much faster rate than cosmic rays. It pulsed the first channel on eight neighboring delay lines simultaneously. An entire crate could be pulsed with sufficient statistics in under 30 minutes. A sample result from these tests is shown in Figure 4.4.

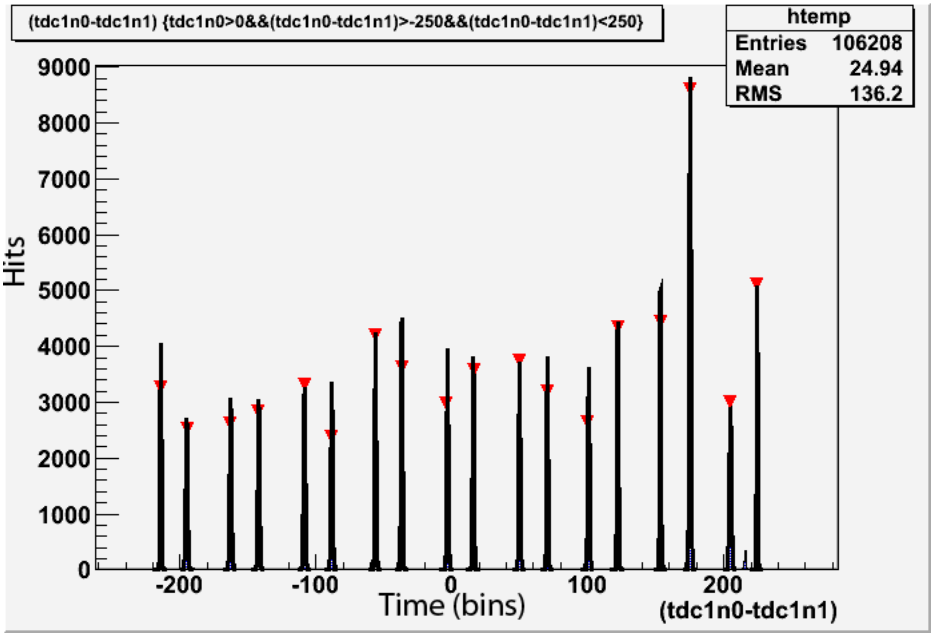

Figure 4.4: Signal-time spectrum of TDC0-TDC1 of pulser data

The pulser data lacks the peak-height signature of the cosmic ray data, as expected, because each wire is being pulsed at the same rate. Pulser data will have 18 peaks on every channel but it also sports another unusual feature. The signal-time spectrum is different than that of the cosmic ray data. The reason for this will be discussed later in the paper.

4.2 Wire Efficiency

The demultiplexed maps are used to create wire based ROOT trees. Data for individual wires becomes the basis for the trees leaves. This allows us to look at single wire efficiencies of seven-wire tracks in the drift chambers (Figure 4.5). What a seven wire track means is that we assume that the fourth wire of the track is the wire that the cosmic ray passed through. This leads to a characteristic pattern on the timing of the three adjacent wires on either side. For example if wire 5 was hit than we would except the drift time of wire 2 to be the smallest drift time of the left three wires. The drift time of wire 2 would be less than wire 3 and wire 3 would be less than wire 4. Of the right three adjacent wires, wire 6 would have the smallest drift time. The drift time of wire 6 would be less than wire 7 and wire 7 would be less than wire 8. There are no requirements on wire 5. If the drift time on wire 5 is found to be zero then this is calculated as an miss, meaning there should have been a hit on this wire but for some reason it is missing in the data.

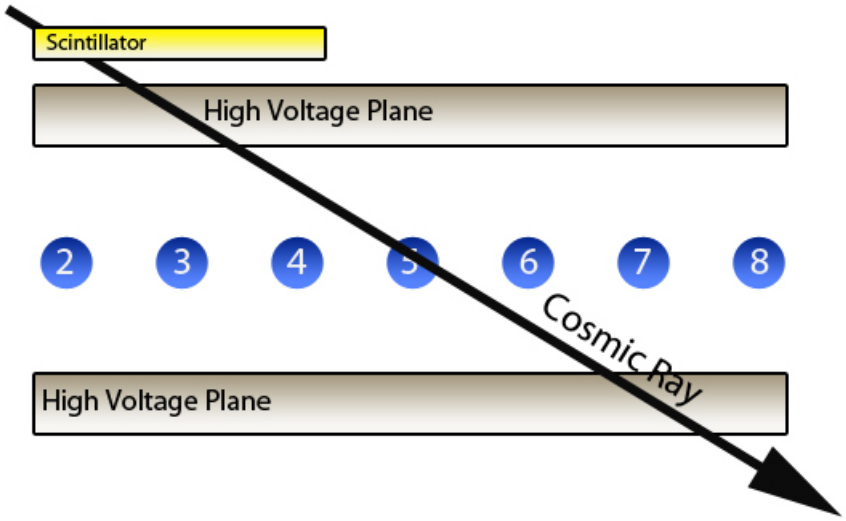

Figure 4.5: Illustration of the requirements on seven-track efficiency for one plane of the drift chamber. $t_2 \leq t_3 \leq t_4$ and $t_6 \leq t_7 \leq t_8$

The above described algorithm was then coded into a ROOT script and run on

demultiplexed data to find suitable track candidates. The script created a text file output of the efficiency results (Figure 4.9) as well as graphs of the efficiency, track candidates and wire hits. The efficiency per wire is defined as Number of Hits / Number of Misses * 100. Summing over all wires allows us to also calculate a total efficiency on the chamber. The script was able to calculate efficiencies for both wire planes (the upper plane's wire numbers were offset by 1000) and limit the event number and wire number. A sample efficiency plot can be seen in Figure 4.6.

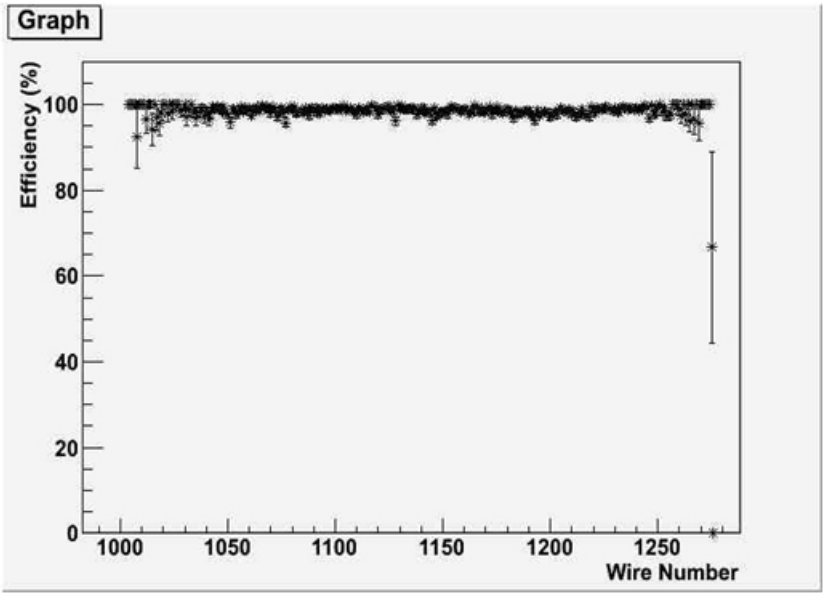

Figure 4.6: Sample efficiency plot of the wires in the upper plane

The calculation of the wire efficiencies served as a diagnostic for the drift chamber performance. This process was able to determine noisy or bad wires that needed to be replaced. The shape of the plot in Figure 4.7 is directly related to the position of the trigger scintillator. The reason behind the shape of the track candidates plot, Figure 4.8, is not fully understood.

4.3 Thermal Tests

Thermal tests were conducted to determine the multiplexing crate's response to temperature changes. Two types of tests were run. The first type was an hour long test to see how the electronics responded to power up. The goal of this test was to see how

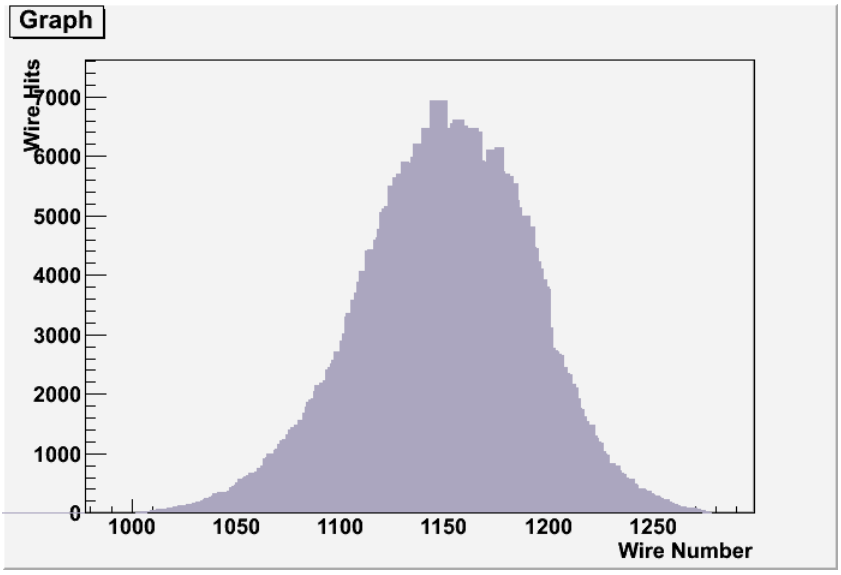

Figure 4.7: A sample plot showing total number of hits per wire in the upper plane

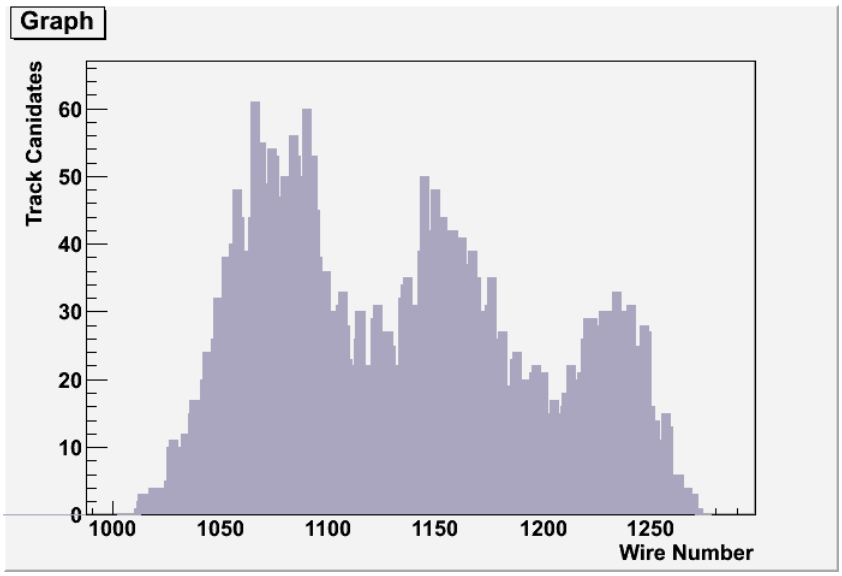

Figure 4.8: A sample plot showing the total number of track candidates per wire in the upper plane.

```
Filename: /home/wmdaq/sxyang/Qweak_1734_R.root
 Channel Range: 1004 to 1276
 **************

Channel Number: tdc1045
 Wire efficiency: 86.363636
 19 out of 22
 Error: 6.799373

Channel Number: tdc1046
 Wire efficiency: 90.000000
 18 out of 20
 Error: 6.363961

Channel Number: tdc1047
 Wire efficiency: 100.000000
 23 out of 23
 Error: 0.000000
```

Figure 4.9: Example of the text output of the efficiency program. TDC means wire number in this case. The offset of 1000 denotes that these are results from the upper wire plane. For example, TDC1045 corresponds to wire 45 in the upper plane.

long it took before the time position of the signals stabilized. The second test was a twenty-four hour test to determine the response of the electronics due to environmental temperature fluctuations. Both types of tests were run to see what kind of constraints had to be put on the validity of the maps. We wanted to know how long we would have to wait after powering up the electronics in order for the peaks to be stable and our map valid. We also wanted to know that over a long data taking period that our map would remain valid. In each case, a single channel was pulsed.

In order to test this, a ROOT script was written that found the location of the signal (peak) at regular time intervals. A Gaussian was then fit to this and the centroid of the fit was graphed versus time. Error on the plotted points was calculated from the error given in the centroid of the Gaussian fit in ROOT. The increments of the time axis were determined by taking the range of the event numbers, dividing that range by time and then multiplying it by the event number step used in the code. For example in the 60 minute thermal run the event range was from event number 2100 to event number 580000, stepping by 1700 events each iteration. This lead to a time separation of approximately 11 seconds between the data points. It should be noted that in all of the graphs the error bars were too small to be seen.

Figure 4.10 shows that there clearly is some initial peak instability upon powering up the electronics. To better locate the stability time the x-axis range was limited to

shortly after the signal locations leveled out. The zoomed in result can be seen in Figure 4.11 . From figure 4.11 we can see that it takes approximately 7 minutes or 400 seconds for the powering up effects to diminish. In total, the peak shift is approximately 200 ps.

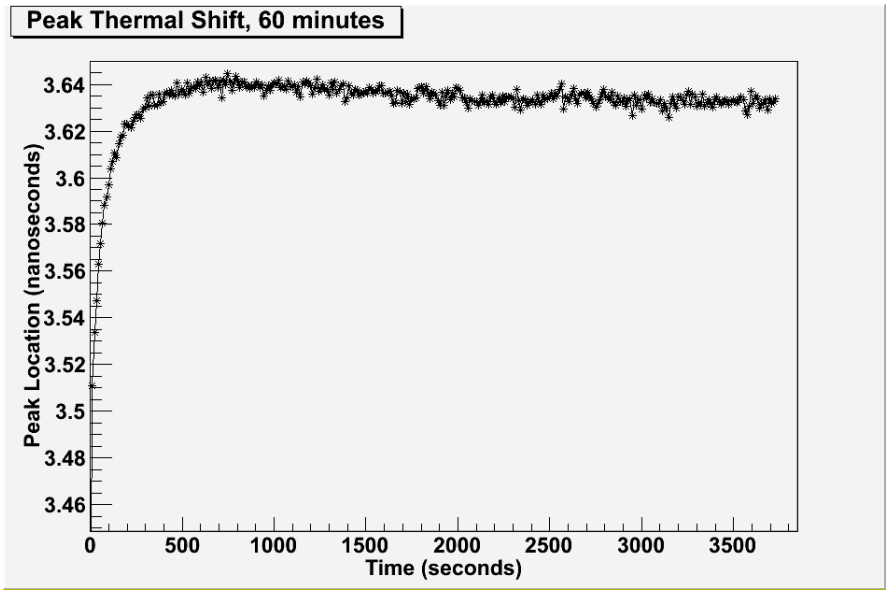

Figure 4.10: Results from the 60 minute thermal run.

This same process was used for the twenty-four hour run. The results, shown in Figure 4.12, were less conclusive because the temperature fluctuations in the building were not monitored. The general drifting of peak location towards smaller values occurs approximately 400 minutes or 7 hours in. This corresponds to approximately 8PM-9PM which qualitatively could correspond to a general decrease in building temperature. It is also not clear from the data whether or not the peak drift begun at 400 minutes reverses itself in the opposite direction or continues towards smaller and smaller values. Unfortunately, the lab had to be moved before longer data runs could be taken. In total the peak shift is approximately 50 ps.

4.4 Peak Shifting Tests

The final part of my research was to explain the difference in the cosmic ray and pulser maps. Initial tests were done to try and determine the source of the effect. It was found that the following did not contribute to the difference in the maps:

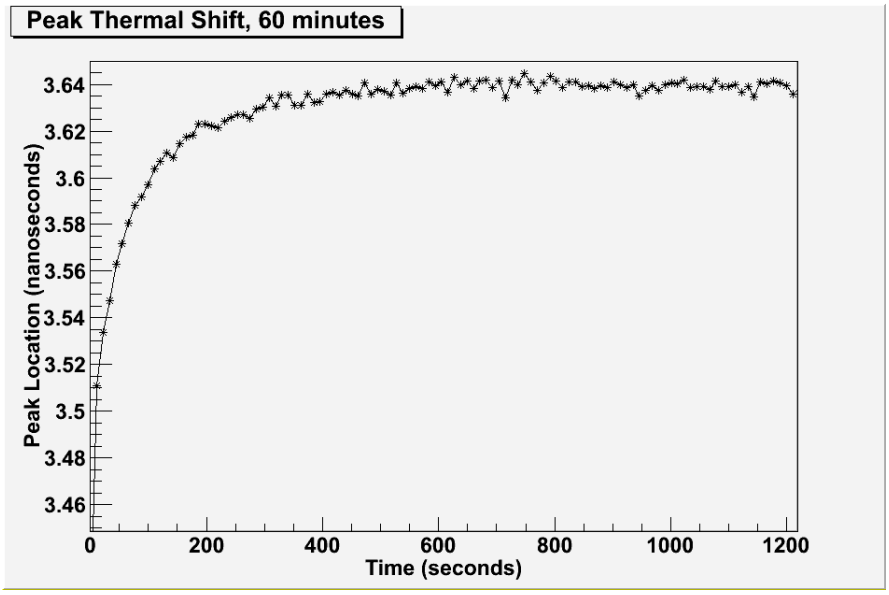

Figure 4.11: Zoomed in results of the 60 minute thermal run.

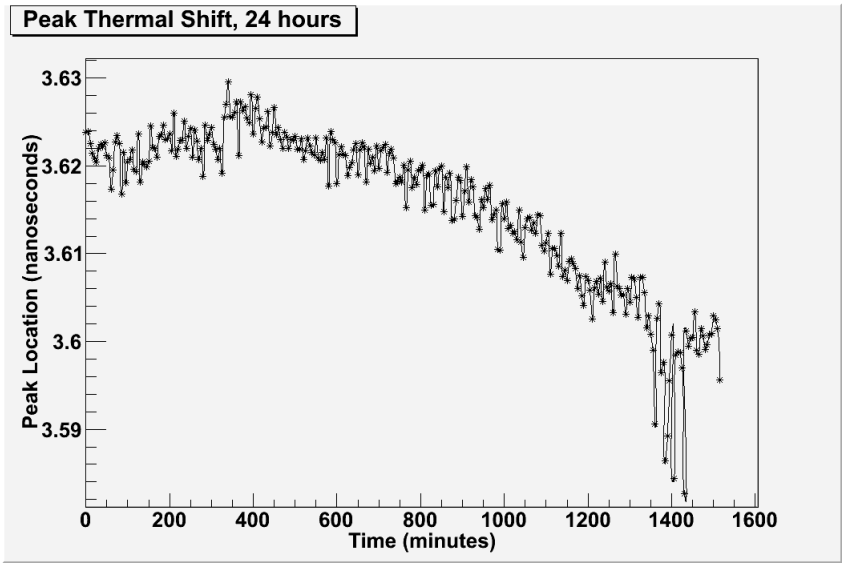

Figure 4.12: Results from the 24hour thermal run. The distance between successive data points is approximately 5 minutes.

- MAD card being used
- pulse size into MAD card
- MAD card threshold
- frequency of pulser
- MUX crate power on/off
- F1 crate power on/off
- amount of delay of signal from gate generator.

Data was then taken using the MAD card pulsed by a function generator for the LVDS pulser, looking at one channel of two delay lines at a time with the intent to look for signs of channel to channel cross-talk. The results of this can be seen in Table 4.1.

Table 4.1: Initial delay tests

Delay Line	Effect
1+2 (1st channel each)	Each was moved, 1 by + 3 bins (112ps) and 2 by - 4 bins
1+3 (1st channel each	Each was moved, 1 by + 5 bins (112ps) and 2 by - 5 bins
1+4 (1st channel each)	None
3+4 (1st channel each)	None
8+1 (1st on, 8 2nd on 1)	None
8+1 (2nd on, 8 3rd on 1)	None
1+2 (1st on 1, 2nd on 2)	Each was moved, 1 by + 7 bins (112ps) and 2 by - 3 bins

The only thing common to all affected channels and different to all the non-affected channels was the delay chip. This is a direct result of the layout of the multiplexing electronics. Figure 3.4 shows that multiple wires are input into a single delay chip, thus if multiple wire signals arrive to the chip within a certain time window this could result in peak shifting. The purpose of further tests were to determine the size of the time window and whether or not this would have an effect on data for the actual experiment.

Initial tests were run by graduate student John Leckey. He tested the MUX crate with a pulse delayed by 1.7 ns, 4.7 ns and 10 ns+. With the 1.7 ns delay he found that the peaks moved by 526.4 ps and 358.4 ps. With the 4.7 ns delay, the peaks moved by 56 ps and 145.6 ps. With the 10+ ns wire, the peaks moved by 33.6 ps and 78.4 ps. His

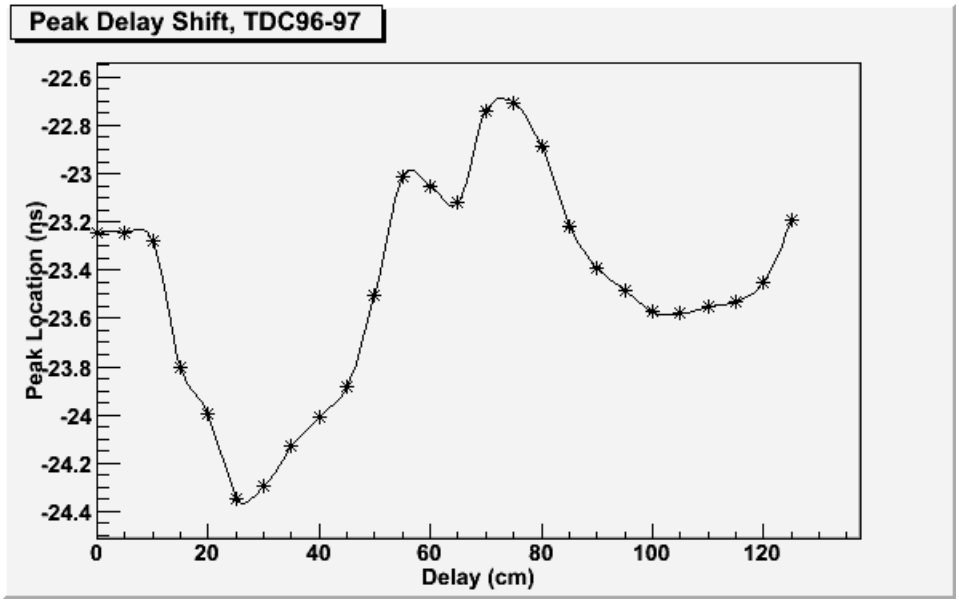

Figure 4.13: Results of the cable delay test on TDC channels 96 and 97.

conclusion was that, the 5 ns delay would still correctly identify peaks using a previous map, based on the map window scheme described in the map making section.

A more rigorous test was developed to determine the exact size of the delay window. The testing procedure was as follows. Two separate lengths of cables were used to pulse channels on the same delay chip. The initial length difference of the cables was sufficient for no effect to be seen. Then one cable was shortened in 5 cm intervals (corresponding to approximately 5 ns of delay) until the effect appeared and then disappeared again.

The results of the tests can been seen in figure 4.13. A total of 125 cm was removed in cable length denoting a total time shift of 12.5 ns. For reasons that will be explained later, it is assumed that the signals arrive within the smallest time window between 60 and 80 cm. Using this as our zero point we can estimate a time window of approximately 40-60 cm in each direction or 4-6 ns. This is in agreement with the preliminary tests.

The shifting RMS plot in Figure 4.14 is used to determine the point in which the signals are arriving almost simultaneously. During preliminary tests it was noticed that with cables of the same length there was cross-talk between the outputs. The signals from neighboring inputs would appear on each other's outputs. The cross-talk would result in a larger RMS value because two peaks are showing up instead of one. This is

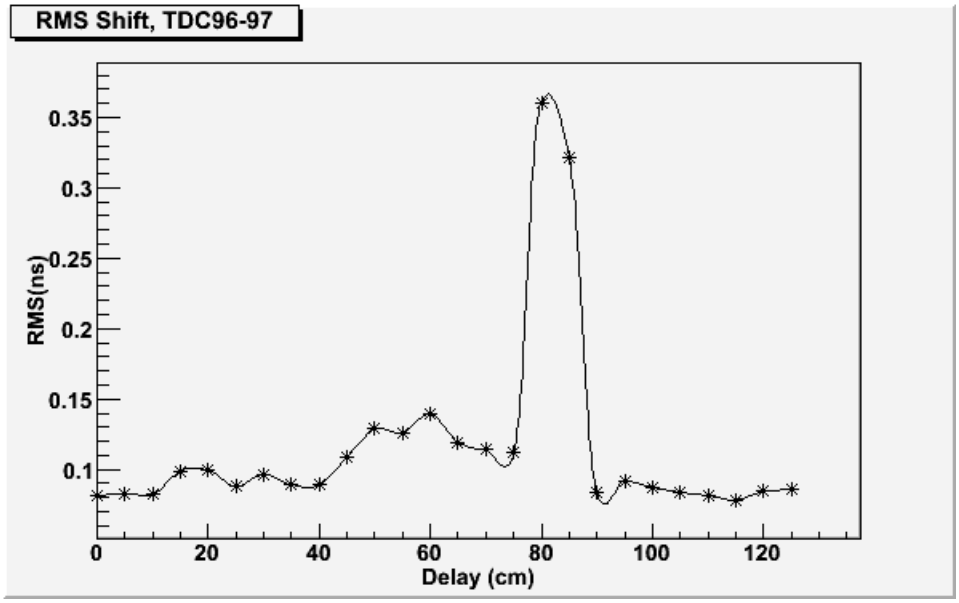

Figure 4.14: The shifting RMS value as the cable length is varied.

how we were able to infer the smallest time separation occurred between 60-80cm. This ghosting effect is described below.

The ghosting effect was first noticed in preliminary tests. The effect is described in the following three figures. In Figures 4.16 and 4.17 channels were pulsed individually, one at a time. For each channel there was a clearly defined single peak. Figure 4.18 shows the result of the same two channels being pulsed at the same time with the same length of cable. It is clear that there are two peaks where there should only be one. It is also clear that the second peak is at the same location in time as it was on it's own individual channel. This is the ghosting effect which occurs when signals arrive at almost exactly the same time.

During the running of the Q-Weak experiment the rate at which particles enter the drift chambers is expected to be on the order of a few kilohertz. This puts the rate on individual wires into the hertz range, (10 Hz * 5 ns = 10^{-8}) and as such the peak shifting effect is expected to be minimal. After my thesis defense, Professor Armstrong wrote an electronic log book entry further discussing the effect on the Q-Weak experiment. This discussion can be found in Appendix A.

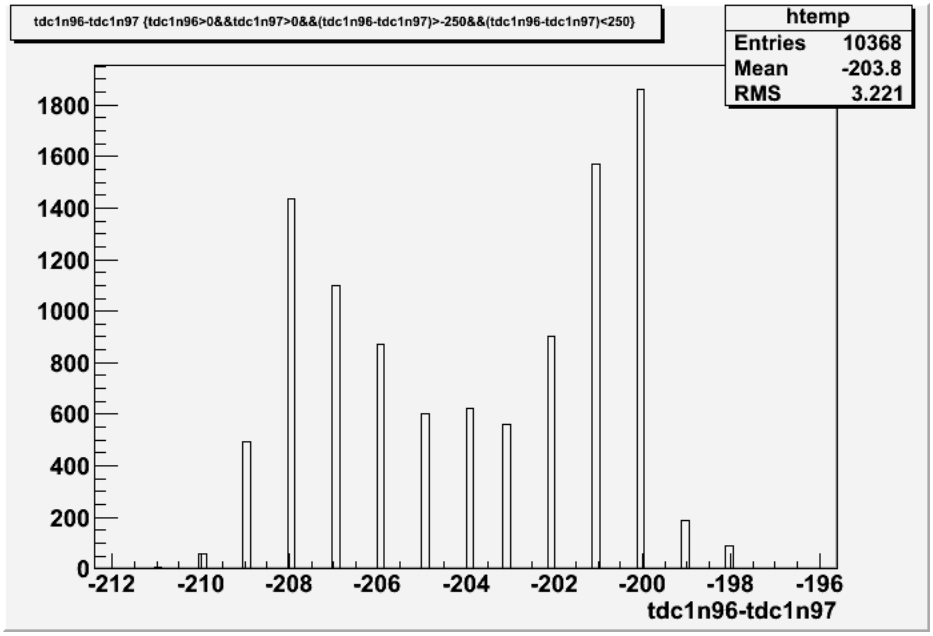

Figure 4.15: Left-Right peak spectrum of the large RMS value, showing two peaks

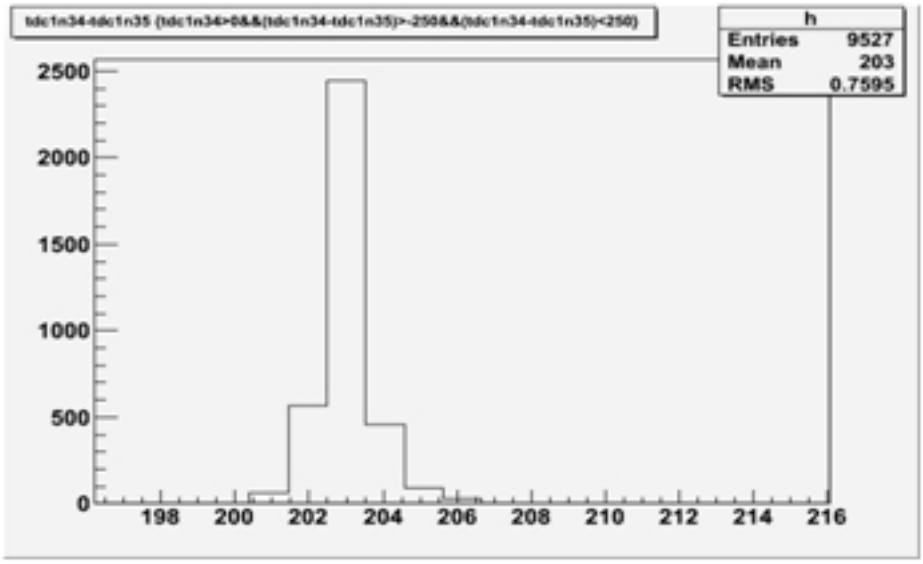

Figure 4.16: Left minus right spectrum with just one channel pulsed.

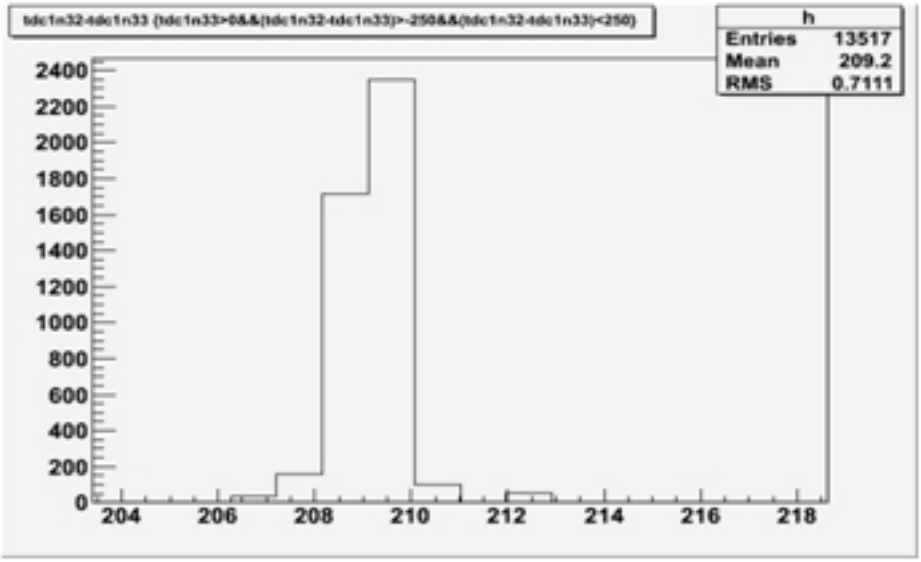

Figure 4.17: Left minus right spectrum with just one channel pulsed.

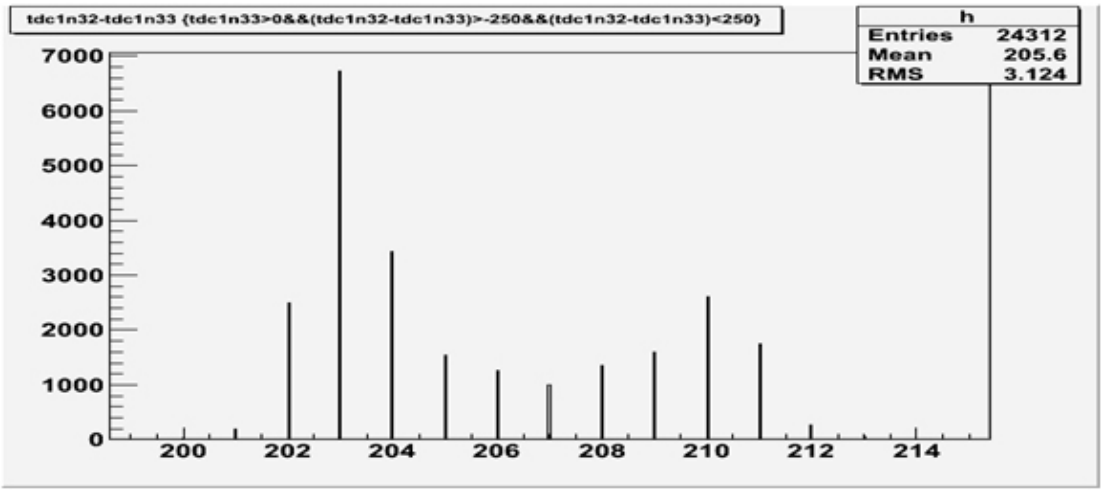

Figure 4.18: Left minus right spectrum with both channels pulsed. When referring to Figures 4.16 and 4.17 it is clear that there is cross-talk (ghosting) between the channels.

Chapter 5

Conclusion

The purpose of my research was to test the multiplexing electronics system that is used to read out data from Q-Weak's vertical drift chambers. Initial tests of the system were conducted at Jefferson Lab, were the electronics were designed and built. These tests included checking the signal integrity, (i.e. that signals appear at the outputs 100% of the time) as well as confirming that signal delay occurred with the specified amount consistently throughout the system. My research built upon these initial tests. Throughout the course of the year I was able to successfully read-out all of the wires from a single drift chamber through the multiplexing crate. I was then able to create a map from this read out that would translate a peak on a channel into a wire number in the chamber. This allowed for the wire data to be demultiplexed and also for seven-track wire efficiencies to be examined. Furthermore, I tested the thermal response of the crate as a result of powering up and over the course of 24 hours. Finally, I elaborated on the reason behind the difference in maps created using a pulser and cosmic ray data. It was found that signals arriving within a 4-6 ns window caused a shift in the location of the signals.

The experiment will use four multiplexing crates to read out all of the data from the four wire chambers. Unfortunately during my time working on the project, only one crate was complete and confirmed working. The remaining three crates are still at Jefferson Lab for testing. Future work, would include running the same tests on these three crates to check their responses to them. Also future work could include a more

rigorous thermal test of the crate run over more than 24 hours to further see how the peaks shifted. Finally, more work could be done with the signal delay tests using longer cables to have more lengths at which there is no shift in the signal's time to confirm without a doubt that the window stated is accurate.

Bibliography

[1] Gerald T. Garvey and Susan J. Seestrom. Parity violation in nuclear physics: A signature of the weak force. *Los Alamos Science*, (21), Nov 1993.

[2] Brian P. Walsh. W&m senior thesis project: "development of a flatness scanner and simulation for qweak wire chambers". *(Unpublished)*, Jan 2007.

[3] W.T.H Van Oers. The qweak experiment: a search for new physics at the tev scale. *Nucl. Phys.*, 805:329c–337c, 2008.

[4] Armstrong et al. The qweak experiment: A search for new physics at the tev scale via the measurement of the protons weak charge. http://www.jlab.org/qweak/, (Unpublished; Proposal to Jefferson Lab Program Advisory Committee) 2001.

[5] Douglas C. Dean. W&m senior honors thesis project: "construction, testing, and characterization of vertical drift chambers for qweak". 2009.

[6] G. Charpak. Application of proportional wire chambers and drift chambers in high-energy physics and other fields. *Nature*, 270(8):479–482, Dec 1977.

[7] F. Sauli. Principles of multiwire proportional and drift chambers, 1977. European Organization for Nuclear Research [CERN].

Appendix A

Discussion of Peak Shifting

The following comments are from the electronic logbook and relate to the peak shifting effect in regards to the overall experiment. The comments were written by Dr. David Armstrong, after the defense of my thesis. It is meant as a continuation of the comments at the end of the Peak Shifting section.

"The wiring of the MUX backplanes is such that three contiguous wires in the chamber tend to be on three sequential delay lines. This means that a typical track will often have three wire hits that pass through the same delay chip. Thus the real question is, given a real track, what is the chance that two time values within 15 ns of each other?"

"Well, at our nominal track angle of around 45 degrees, the time spacing of hits from adjacent wires should be something of order 100 ns. So, adjacent wires should not (in general) have a problem. However, this is not the case when the track crosses the wire plane, since a perfectly symmetric track which crosses the mid-plane exactly between two wires would have exactly the same drift time for the pairs of wires, i.e. in a 6-wire track, the drift times for the pairs (1,6) and (2,5) and (3,4) should be the same. The issue then would be the pair (3,4) which are on adjacent delay lines, and so are likely to share the same delay chip. Estimating the probability of a pair like this having hits within the 15 ns window is hard to do "back on the envelope", since it depends on the track angle distribution, etc."